

# OceanNet: A principled neural operator-based digital twin for regional oceans

Ashesh Chattopadhyay<sup>1\*</sup>, Michael Gray<sup>2</sup>, Tianning Wu<sup>2</sup>, Anna B. Lowe<sup>2</sup> and Ruoying He<sup>2\*</sup>

<sup>1\*</sup>Applied Mathematics, University of California, Santa Cruz, Santa Cruz, 95060, California, United States.

<sup>2</sup>Marine, Earth & Atmospheric Sciences, North Carolina State University, Raleigh, 27695, North Carolina, United States.

\*Corresponding author(s). E-mail(s): [aschatto@ucsc.edu](mailto:aschatto@ucsc.edu);  
[rhe@ncsu.edu](mailto:rhe@ncsu.edu);

Contributing authors: [magray@ncsu.edu](mailto:magray@ncsu.edu); [twu27@ncsu.edu](mailto:twu27@ncsu.edu);  
[ablowe@ncsu.edu](mailto:ablowe@ncsu.edu);

## Abstract

While data-driven approaches demonstrate great potential in atmospheric modeling and weather forecasting, ocean modeling poses distinct challenges due to complex bathymetry, land, vertical structure, and flow non-linearity. This study introduces OceanNet, a principled neural operator-based digital twin for ocean circulation. OceanNet uses a Fourier neural operator and predictor-evaluate-corrector integration scheme to mitigate autoregressive error growth and enhance stability over extended time scales. A spectral regularizer counteracts spectral bias at smaller scales. OceanNet is applied to the northwest Atlantic Ocean western boundary current (the Gulf Stream), focusing on the task of seasonal prediction for Loop Current eddies and the Gulf Stream meander. Trained using historical sea surface height (SSH) data, OceanNet demonstrates competitive forecast skill by outperforming SSH predictions by an uncoupled, state-of-the-art dynamical ocean model forecast, reducing computation by 500,000 times. These accomplishments demonstrate the potential of physics-inspired deep neural operators as cost-effective alternatives to high-resolution numerical ocean models.

**Keywords:** Data-driven model, ocean forecasting, neural operator, spectral bias

# 1 Introduction

An essential component of the Earth’s ocean circulation is the northern Atlantic Ocean’s western boundary current (WBC) system, which includes the Loop Current (LC), Loop Current eddies (LCE), the Gulf Stream (GS), and Gulf Stream meander (GSM). The WBC plays a critical role in the transport of heat, salt, and nutrients, and strongly influences global weather, climate, and marine ecosystems. Recent studies have shown the promise of using data-driven approaches to model and predict atmospheric circulation, but complexities in the ocean system present additional challenges when building data-driven models [1–3]. One challenge is the complex land boundaries, such as in the Gulf of Mexico (GoM). Equally difficult to model, the GS frequently sheds eddies as a result of nonlinear flow and the interactions of cool, subpolar circulation from the north and warm, subtropical circulation from the south. Predicting LCEs in the GoM and GS meander and eddy separation have been long-standing challenges for numerical ocean models [4–6]. The separation mechanism involves nonlinear barotropic and baroclinic instabilities of ocean currents, complex flow-topography interactions, and, in the case of the GS, interaction with the Deep Western Boundary Current [7–10]. These challenging features require carefully calibrated, high-resolution numerical models and tremendous computing resources to resolve [11–13].

Recent efforts in emulating ocean dynamics with deep learning-based approaches have primarily focused on predicting large-scale circulation features, such as those resolved by empirical orthogonal functions (EOFs) [14] or on constructing low-dimensional representations [15]. However, there has yet to be a comprehensive data-driven model for the ocean akin to those used in global atmospheric modeling.

Data-driven modeling in Earth sciences has focused on predicting global atmospheric dynamics [1–3, 16, 17]; weather prediction has been used as a benchmark. The primary advantage of data-driven models lies in their computational efficiency, enabling the execution of a large number of ensembles. This facilitates seamless and efficient data assimilation leading to improved estimates of extreme weather events. Several recent studies [1–3] have demonstrated that these data-driven models can achieve accuracy comparable to, and often surpassing, state-of-the-art numerical weather prediction models such as the Integrated Forecasting System (IFS), at a significantly reduced computational cost. This achievement holds substantial promise for incorporating deep learning-based data-driven models into the suite of operational weather forecasting models.

A significant limitation of these models arises when they are integrated over longer time scales ( $\geq 2$  weeks), leading to instability and the emergence of nonphysical features (see Fig. 1 in Chattopadhyay et al. [18]). The cause of this instability was identified as “spectral bias” [18], an inductive bias in *all* deep neural networks that hinders their ability to capture small-scale features in turbulent flows. A potential solution was proposed in [18] in the form

of a framework to construct long-term stable digital twins for atmospheric dynamics.

Research into data-driven digital twins for both global and regional ocean modeling is still in its infancy and has not been explored to the same extent as in atmospheric modeling. The development of long-term stable, accurate data-driven ocean models that maintain computational efficiency is essential for realizing data-driven digital twins for the entire Earth system.

We present here a principled neural operator-based digital twin for the northwest Atlantic Ocean's western boundary current, built upon the same principles as the FouRK model introduced in Chattopadhyay *et al.* [18]. The proposed model, OceanNet, relies on a Fourier neural operator (FNO), which incorporates a predictor-evaluate-corrector (PEC) integration scheme to suppress autoregressive error growth. Additionally, a spectral regularizer is employed to mitigate spectral bias at small scales.

OceanNet is trained on historical sea surface height (SSH) data from a high-resolution northwest Atlantic Ocean reanalysis and demonstrates remarkable stability and competitive skills. It often outperforms SSH prediction made by the state-of-the-art Regional Ocean Modeling System (ROMS) while maintaining a computational cost that is 500,000 cheaper. This marks the first instance of a fully data-driven ocean model exhibiting competitive or superior performance in predicting high-resolution SSH fields compared to a state-of-the-art numerical ocean model. This achievement underscores the potential of structured, physics-inspired deep neural operators as a cost-effective alternative to computationally expensive high-resolution numerical models.

## 2 Results

Mesoscale ocean circulation dynamics can be well represented by the spatio-temporal evolution of SSH fields. In this section we conduct a comprehensive comparison of SSH predictions generated by OceanNet and the dynamical ROMS forecast with independent reanalysis data. To assess the performance rigorously, we employ both qualitative and quantitative measures. The metrics for evaluating predictive accuracy of SSH include root mean squared error (RMSE) and correlation coefficient (CC), which are widely recognized and employed in forecasting [1–3, 18]. In addition, we incorporate a specialized object-tracking metric to evaluate the prediction of major ocean features delineated by SSH contours: the modified Hausdorff distance (MHD, [19]). MHD quantifies the comparison of predicted eddy/meander structures to their counterparts in the reanalysis data; identical shapes have an MHD of zero. To provide a comprehensive assessment, we also present qualitative snapshots of the predicted SSH fields generated by OceanNet, ROMS dynamical forecast, and the independent SSH field derived from the reanalysis.

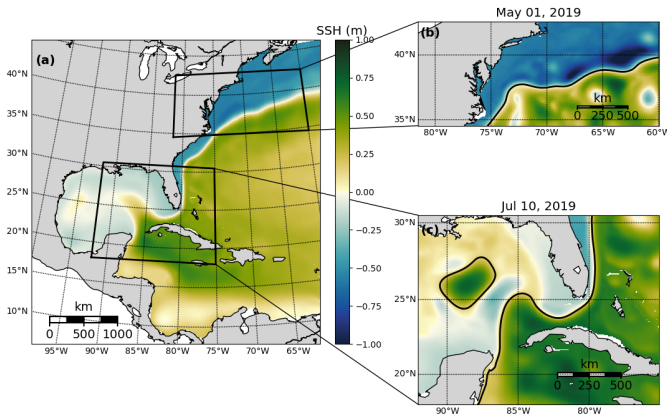


**Fig. 1** The domain for the reanalysis data covering the northwestern Atlantic (a). The two subdomains used to develop OceanNet, specifically (b) the GS separation from the central US east coast to  $60^{\circ}\text{W}$  and (c) the LC eddy-shedding region in the eastern GoM, extending from  $92^{\circ}\text{W}$  into the Atlantic  $75^{\circ}\text{W}$ . The mean SSH from 1993-2020 in the reanalysis data is shown in (a), while (b) and (c) depict daily mean SSH on May 1, 2019, and July 10, 2019, respectively. All three domains share the same color scale.

## 2.1 Performance of OceanNet in the GoM

We present an evaluation of OceanNet’s seasonal (up to 120 days) forecasting performance compared to that of a ROMS forecast for two major GoM LCE shedding events: Eddy Sverdrup (Jul 2019-Jan 2020) and Eddy Thor (Jan 2020 - Sep 2020). The target LC dynamics, represented by spatio-temporal evolutions of SSH, are from the reanalysis dataset. Specifics regarding the generation and structure of the reanalysis dataset are covered in section 4.1.

A qualitative assessment (Fig. 2) reveals that OceanNet excels in capturing the dynamics of LC eddy shedding and reattachment, outperforming the ROMS dynamical forecasts for these two events. Furthermore, OceanNet maintains both stability and physical consistency for at least 120 days. For this domain, OceanNet is trained with a 5-day lead, consistent with the LC and LCE evolution timescale. ROMS predictions were initialized five days apart to allow for fair comparisons between the two models. OceanNet predictions have a “wall-clock” execution time of microseconds, approximately 500,000 times faster than ROMS dynamical forecasts.

An examination of RMSE, CC, and MHD for SSH, over a 120-day period (Fig. 3) demonstrates that OceanNet is consistently competitive or better than ROMS dynamical forecasts, and outperforms random predictions (indicated by the horizontal dashed lines). These random predictions are derived from 1,000 random pairs of samples from the training data covering the period

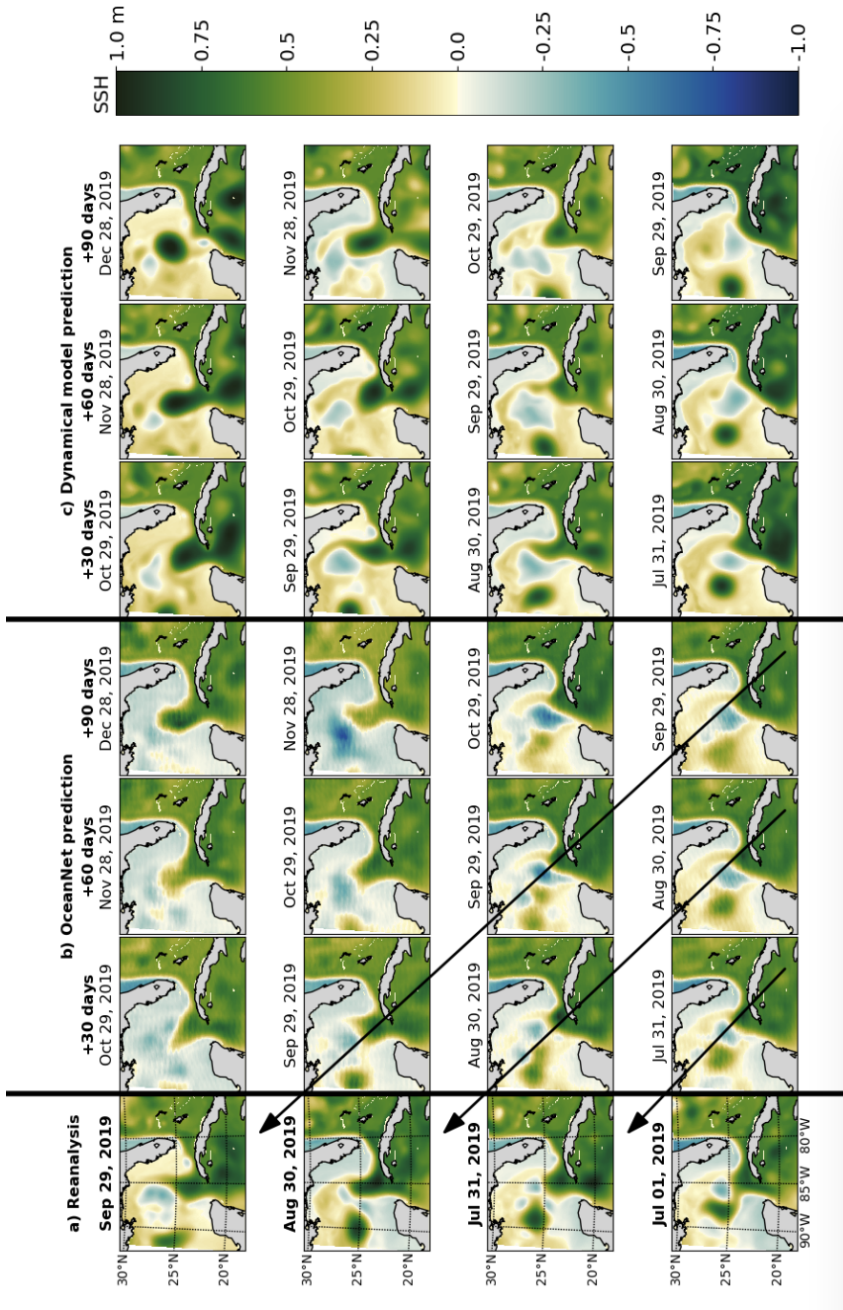


**Fig. 2** Prediction performance of OceanNet. (a) SSH fields from the ocean reanalysis. (b) Predicted SSH generated by the OceanNet. (c) ROMS dynamical forecasts. Each row in the OceanNet and dynamical model predictions was initialized with the corresponding reanalysis data in the left column. The predictions display SSH forecasts for 30, 60, and 90 days. To evaluate the predictions, we can examine a diagonal comparison with the reanalysis SSH, as indicated by the black arrows in (b). The same diagonal comparison can be conducted with the ocean reanalysis data for (c).

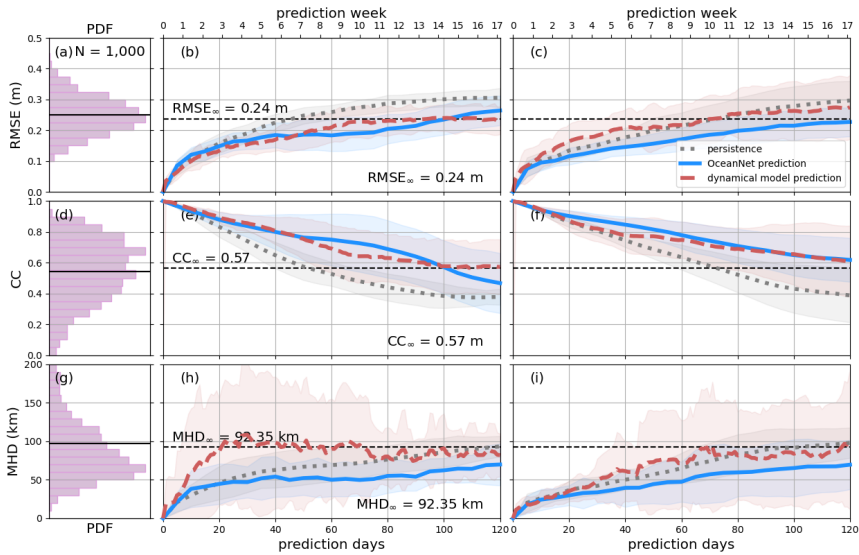


**Fig. 3** OceanNet performance metrics in the GoM: RMSE (a-c), CC (d-f), and MHD (g-i). In the left column, probability density functions (PDFs) are presented for 1,000 random pairs sourced from the training data spanning 1993-2018 (means shown by black horizontal lines). The performance statistics, calculated based on forecasts of 0-120 days for eddies Sverdrup (middle column) and Thor (right column), are displayed as mean values (lines) with standard deviations (shading). The black horizontal dashed lines in these columns denote saturation values determined as 95% of the means derived from the random pairs. In the middle and right columns, solid blue lines are OceanNet, dashed red lines are the ROMS dynamical forecast model, and gray dots are persistence. These representations illustrate how each method's statistics compare with the target SSH from the reanalysis dataset

of 1993-2018 to calculate the saturation values, which quantify the intrinsic predictability of the ocean system [20–22]. Comparing OceanNet and ROMS with persistence forecasting, we see that ROMS suffers from inaccuracies in predicting the timing and configuration of the eddy-shedding and reattachment process, and thus underperforms persistence forecast on several occasions. This is not the case for OceanNet.

We conducted a further comparison (Supplementary Information) of OceanNet with previous deep learning-based models that have been successfully used in weather prediction, such as the model introduced by Weyn et al. [23]. The spectral characteristics of these models exhibit deviations in the high wavenumbers, rendering their predictions unphysical beyond a 2-week forecasting horizon (Fig. S1). A geostrophic constraint within the loss function was also tested (Fig. S2), but OceanNet in its current design performed better.

## 2.2 Performance of OceanNet in the North Atlantic GS Region

We present qualitative and quantitative evaluations of OceanNet’s forecasting performance compared to the ROMS dynamical model forecast for GSM in the northwest Atlantic. OceanNet was specifically trained for this domain with a lead time of 4 days to resolve the evolution of the northern boundary of the GS. To ensure alignment with the initialization dates for ROMS (which were separated by 5 days), we show the 20th, 40th, and 60th-day forecasts, as opposed to the 30th, 60th, and 90th-day forecasts used for the LC.

A qualitative assessment reveals that OceanNet effectively captures the SSH propagation of undulations in the northern boundary of the GS. Moreover, it skillfully captures large-scale eddies traveling into and out of the domain, even without receiving any boundary information (Fig. 4). In contrast, ROMS dynamical model forecast tends to overpredict extreme values of SSH and the meridional amplitude of the northern boundary. While it is sensitive to initial conditions, OceanNet remains physically consistent over long-term forecasts in this region as well. As observed in the GoM, OceanNet provides stable and physically reasonable SSH predictions for the GSM for at least 120 days (not shown for brevity).

Similar to the GoM, OceanNet consistently outperforms ROMS in RMSE, CC, and MHD computed between the predicted SSH values and the reanalysis SSH over 120 days (Fig. 5). Persistence forecasting also fares reasonably well in this region due to the background state of the GSM; however, OceanNet still outperforms persistence in all three metrics over 120 days.

## 3 Discussion

In this study, we introduce OceanNet, a deep neural operator, with principled design structures within the architecture, to function as a digital twin for long-term (up to 120 days) mesoscale ocean circulation forecasting. Our major technical contributions encompass the development of an FNO and the application of a PEC-based convergent integration scheme, along with a spectral regularizer. Together, these techniques mitigate autoregressive error growth and the small-scale spectral bias frequently observed in data-driven models of multi-scale dynamical systems.

By training the model on 26 years (1993-2018) of high-resolution regional ocean reanalysis data for the northwest Atlantic, we evaluate OceanNet’s ability to predict mesoscale ocean processes such as the GoM LC eddy shedding and GSM over a 90-120 day forecasting horizon. OceanNet demonstrates remarkable stability and consistently outperforms the ROMS dynamical ocean forecast while being 500,000 times faster. These results demonstrate the potential of utilizing scientific machine learning to develop long-term stable, and accurate data-driven ocean models of great computational efficiency, paving the way for realizing a data-driven digital twin encompassing the entire climate system.

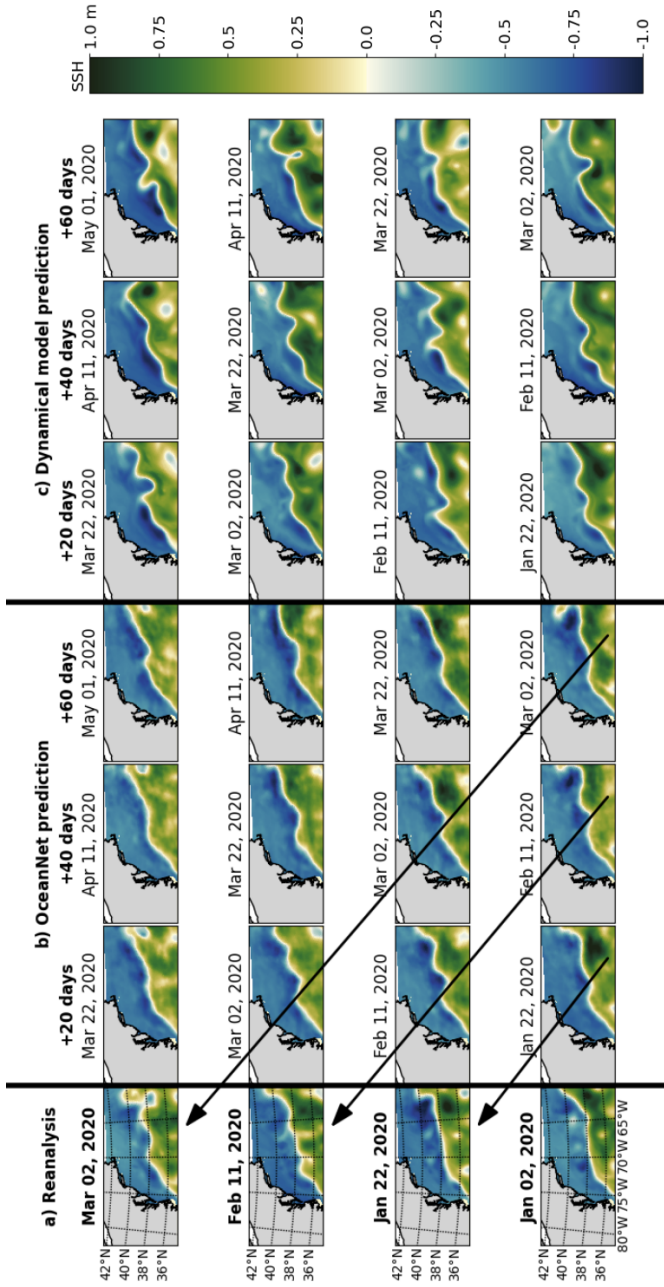


**Fig. 4** Performance of OceanNet for GS prediction. (a) SSH fields from the ocean reanalysis. (b) Predicted SSH generated by OceanNet. (c) ROMS dynamical model forecasts. In both OceanNet and dynamical model predictions, each row was initialized with the corresponding reanalysis data in the left column. SSH forecasts are provided for 20, 40, and 60 days. To evaluate the predictions, we can perform a diagonal comparison with the reanalysis SSH, as indicated by the black arrows in (b). The same diagonal comparison can also be conducted with the ocean reanalysis data for (c).

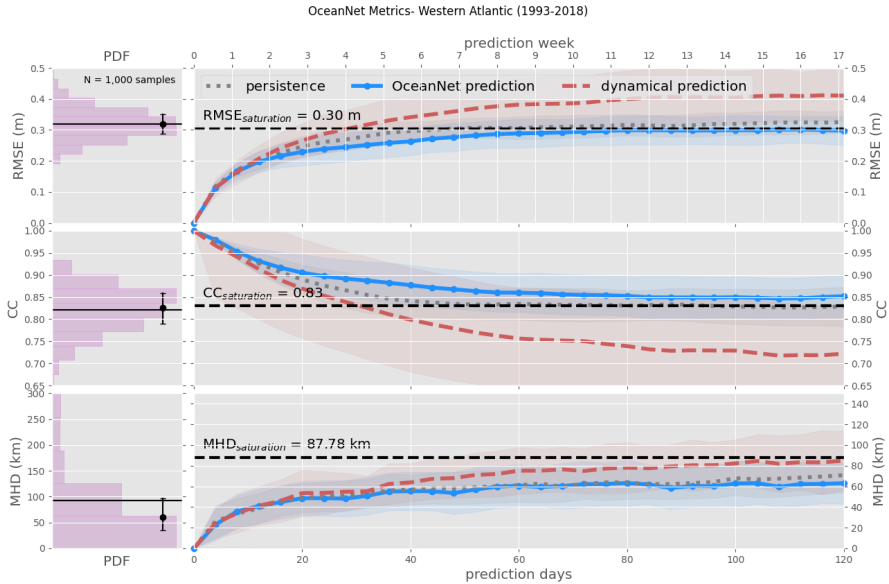


**Fig. 5** OceanNet’s performance metrics in the northwest Atlantic: RMSE (top), CC (middle), and MHD (bottom), compared to the persistence forecast and ROMS dynamical model forecast. In the left column, probability density functions (PDFs) are presented, derived from 1,000 random pairs sourced from the training data spanning 1993-2018 (means shown by black horizontal lines). The performance statistics, calculated based on forecasts of 0-120 days, are displayed as mean values (lines) with standard deviations (shading). The black horizontal dashed lines denote saturation values, which are determined as 95% of the means derived from the random pairs. Solid blue lines are OceanNet, dashed red lines are the ROMS dynamical forecast model, and gray dots are persistence. These representations illustrate how each method’s statistics compare with the target SSH from the reanalysis dataset

Despite the promising forecast accuracy observed with reanalysis data, our algorithm possesses several limitations. First, this study exclusively trained and tested OceanNet using reanalysis data pertaining to mesoscale ocean eddies and meanders. Real-world ocean forecasting systems operate with dynamical ocean models and real-time ocean observational data, covering dynamic processes across diverse spatial scales. The disparities between these data sources and scales necessitate further investigation into OceanNet’s performance across various ocean applications. Second, OceanNet’s focus is solely on SSH. This study did not explore other ocean state variables, such as currents and temperature. The omission of these variables may restrict the model’s capacity to accurately predict small-scale ocean circulation phenomena, such as shelf break jets and frontal currents. Third, AI-based methods frequently produce smoother forecast results than dynamical models, which can potentially lead to an underestimation of the magnitudes of extreme ocean events. Therefore, additional research is imperative to assess OceanNet’s performance under extreme ocean conditions, e.g., during severe storms.

Significant opportunities exist for improvement in both AI-based methods and dynamical model-based ocean forecasting. In the AI domain, potential advancements involve the integration of subsurface ocean states and additional ocean variables, the incorporation of temporal dimensions through the training of four-dimensional deep networks, and the exploration of more complex network architectures with increased depth and breadth. In the realm of numerical ocean forecast modeling, the development of pre- and post-processing techniques can help mitigate the inherent biases found in ocean models. We expect that a hybrid approach, combining data-driven and dynamical numerical models will play a pivotal role in pushing the boundaries of excellence in ocean prediction.

## 4 Data and Methods

### 4.1 Reanalysis Data

We utilized high-resolution northwest Atlantic regional ocean reanalysis data to train OceanNet. This reanalysis was generated using ROMS with the ensemble Kalman filter data assimilation method (EnKF). It features a horizontal resolution of 4 km with 50 vertical layers. For surface atmospheric forcing, we employed data from the European Center for Medium-Range Weather Forecasting (ECMWF) Reanalysis v5 (ERA5), while open boundary conditions were derived from the Copernicus Global Ocean Physics Reanalysis (GLO-RYS). Ten major tidal constituents from the OSU TPXO tide database were used. The model incorporated 120 river inputs, sourced from the National Water Model and climatology datasets. The temporal scope of the reanalysis spans from January 1, 1993 to December 31, 2020, with daily output.

The assimilated observations encompass a variety of sources, including AVHRR and MODIS Terra sea surface temperature, AVISO along-track sea surface height anomaly, glider temperature/salinity observations from the Integrated Ocean Observing System (IOOS), and the EN4 dataset which aggregates data from Argo floats, shipboard surveys, drifters, moorings, and other sources. EnKF assimilates data with no influence or retainment of previous timesteps, as opposed to 3D/4D-var methods, which include forward and backward passes over the results to ensure continuity. The resulting data assimilative ocean reanalysis allows us to train OceanNet with a time-space continuous SSH dataset with no external knowledge (as would be the case for observations).

OceanNet is trained on 5-day mean SSH data with a 5-day lead time for the GoM domain and 4-day lead time for the GSM domain. Both training datasets consist of 26 years of reanalysis data from 1993 through 2018. SSH Forecasting was conducted for 2019-2020. Further details on OceanNet's training process are provided in section 4.2.

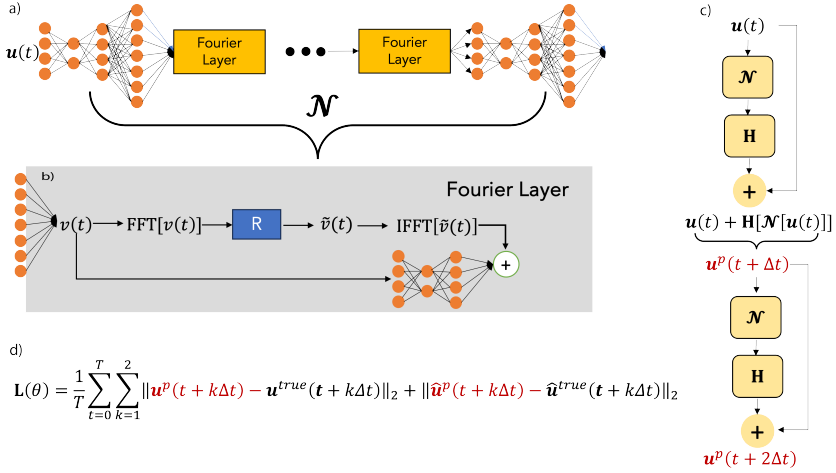


**Fig. 6** (a) A schematic of the OceanNet model. (b) The Fourier Neural Operator, depicted as  $\mathcal{N}$ . (c) 2-time-step training scheme. (d) The loss function used. Here,  $u$  is the state of the system that is predicted, and  $H$  is the PEC-based convergent integration scheme used.

## 4.2 OceanNet: Configuration and Design

The OceanNet model (Fig. 6) has three major components. the Fourier Neural Operator (FNO), which is used to learn the residual, similar to Krishnapriyan *et al.* [24] and Chattopadhyay *et al.* [18]; the PEC integrator; and the spectral regularizer, which alleviates spectral bias.

### 4.2.1 Fourier Neural Operator (FNO)

OceanNet is built upon the FNO [25]. Training utilizes labeled pairs of historical 5-day mean SSH data in the GoM (section 4.1),  $X(t)$  (input),  $X(t + 5\Delta t)$  (label), and  $X(t + 10\Delta t)$  (label), where  $\Delta t = 1$  day. For training OceanNet in the northwest Atlantic region, the labels are  $X(t + 4\Delta t)$  and  $X(t + 8\Delta t)$ . The training assumes the governing partial differential equation for the reduced ocean system involves ocean states  $X(t)$ :

$$\frac{d\mathbf{X}}{dt} = \mathbf{F}(\mathbf{X}(t)). \quad (1)$$

To integrate the system from the initial condition,  $\mathbf{X}(t)$ , we represent Eq. (1) in its discrete form:

$$\mathbf{X}(t + 5\Delta t) = \underbrace{\mathbf{X}(t)}_{\mathbf{H}[\circ]} + \underbrace{\int_t^{t+5\Delta t} \underbrace{\mathbf{F}(\mathbf{X}(t))}_{\mathcal{N}[\circ, \theta]} dt}_{\mathbf{H}[\circ]}. \quad (2)$$

Here,  $\mathcal{N}$  is an FNO that parameterizes  $\mathbf{F}$  with four Fourier layers, similar to Li et al. [25], each layer retaining 64 Fourier modes.  $\theta$  represents the  $\approx 80 \times 10^6$  trainable parameters of the FNO.  $\mathbf{H}$  is a higher-order predictor–evaluate–corrector (PEC) integrator (section 4.2.2).

### 4.2.2 Predictor-Evaluate-Corrector Integration Scheme

Similar to the higher-order integration scheme in the form of fourth-order Runge-Kutta (RK4) (Chattopadhyay et al. [18]), we implement a PEC scheme in OceanNet, represented by the operator,  $\mathbf{H}$ . The operations in  $\mathbf{H}$  are given by:

$$i_1 = \mathcal{N}[\mathbf{X}(t), \theta], \quad (3a)$$

$$z = \mathbf{X}(t) + \mathcal{N}\left[\mathbf{X}(t) + \frac{1}{2}i_1, \theta\right]. \quad (3b)$$

The predicted state is given by  $z = \mathbf{H}[\mathcal{N}(\mathbf{X}(t)), \theta]$ .

Although most of the higher-order integration schemes, including RK4, demonstrate good performance for this problem, we have identified PEC as the most effective choice. A theoretical study of the effect of each integration scheme on the inductive bias of the trained  $\mathcal{N}$  is an active area of research [24], especially for understanding the role it plays on the subsequent spectral bias (section 4.2.3).

### 4.2.3 Fourier Regularizer and 2-time-step Loss Function

In OceanNet’s loss function, we incorporate a spectral regularizer based on Fourier transforms introduced in Chattopadhyay et al. [18]. This is in addition to the standard mean squared error loss (MSE) function, which is computed exclusively for grid points located over the ocean.

The spectral regularizer penalizes deviations in the absolute value of the latitude-averaged zonal Fourier spectrum (Fourier spectrum from now on) of the SSH field at small wavenumbers. Such deviations arise due to spectral bias [18, 26], which represents an inherent inductive bias in deep neural networks. This bias is responsible for their limitations in learning the fine-scale dynamics of turbulent flow.

Furthermore, the combined loss function, which integrates both MSE and the spectral regularizer is evaluated over two time steps, namely  $t+5\Delta t$  ( $t+4\Delta t$

for GS) and  $t + 10\Delta t$  ( $t + 8\Delta t$  for GS), to extend the stability horizon. This two-time-step loss function had remarkable success in the weather prediction model, FourCastNet [1]. The spectral regularizers for time  $t + 5\Delta t$  and  $t + 10\Delta t$  are defined as follows:

$$\mu(t + 5\Delta t, \theta) = \sum_{t=0}^{t=T} \left\| \widehat{\mathbf{X}}(t + 5\Delta t) \Big|_{k_x \geq k_T} - \widehat{\mathbf{H}}[\mathcal{N}(\mathbf{X}(t), \theta)] \Big|_{k_x \geq k_T} \right\|_2^2. \quad (4)$$

$$\mu(t + 10\Delta t, \theta) = \sum_{t=0}^{t=T} \left\| \widehat{\mathbf{X}}(t + 10\Delta t) \Big|_{k_x \geq k_T} - \widehat{\mathbf{H}}[\mathbf{H}[\mathcal{N}(\mathbf{X}(t), \theta)]] \Big|_{k_x \geq k_T} \right\|_2^2. \quad (5)$$

Here, the  $[\widehat{\circ}]$  operator is the latitude-averaged zonal Fourier transform of both the predicted and the target SSH fields.  $k_T$  is a cutoff wavenumber chosen to be 100 after significant trial and error. The loss functions for  $t + 5\Delta t$  and  $t + 10\Delta t$  are given by  $\mathbf{L}(t + 5\Delta t, \theta)$ :

$$\mathbf{L}(t + 5\Delta t, \theta) = \sum_{t=0}^{t=T} \|\mathbf{X}(t + 5\Delta t) - \mathbf{H}[\mathcal{N}(\mathbf{X}(t), \theta)]\|_2^2 + \lambda\mu(t + 5\Delta t, \theta). \quad (6)$$

$$\mathbf{L}(t + 10\Delta t, \theta) = \sum_{t=0}^{t=T} \|\mathbf{X}(t + 10\Delta t) - \mathbf{H}[\mathbf{H}[\mathcal{N}(\mathbf{X}(t), \theta)]]\|_2^2 + \lambda\mu(t + 10\Delta t, \theta). \quad (7)$$

The total loss is given by:

$$\mathbf{L}(\theta) = \mathbf{L}(t + 5\Delta t, \theta) + \mathbf{L}(t + 10\Delta t, \theta). \quad (8)$$

The spectral regularizer ensures that the high wavenumbers in the Fourier spectrum of SSH remain consistent with the target Fourier spectrum. This measure is effective in reducing spectral bias throughout the training process. The two-time-step loss function enhances the stability horizon of the model. The number of time steps over which the loss is calculated can potentially be extended. However, with each increase in the number of time steps, the memory requirement for the subsequent backpropagation process during training grows exponentially.

**Acknowledgments.** We thank Subhashis Hazarika and Maria Molina for the insightful discussions and Jennifer Warrillow for editorial assistance. MG, AL, TW, and RH, were supported by NSF awards 2019758 and 2331908. AC performed partial work at the Palo Alto Research Center, SRI International. All

authors contributed equally to the research conducted and the writing of the paper. The codes used in this study will be made available upon publication.

## References

- [1] Pathak, J., Subramanian, S., Harrington, P., Raja, S., Chattopadhyay, A., Mardani, M., Kurth, T., Hall, D., Li, Z., Azzizadenesheli, K., et al.: FourCastNet: A global data-driven high-resolution weather model using adaptive Fourier neural operators. arXiv preprint arXiv:2202.11214 (2022)
- [2] Lam, R., Sanchez-Gonzalez, A., Willson, M., Wirnsberger, P., Fortunato, M., Pritzel, A., Ravuri, S., Ewalds, T., Alet, F., Eaton-Rosen, Z., et al.: Graphcast: Learning skillful medium-range global weather forecasting. arXiv preprint arXiv:2212.12794 (2022)
- [3] Bi, K., Xie, L., Zhang, H., Chen, X., Gu, X., Tian, Q.: Accurate medium-range global weather forecasting with 3d neural networks. *Nature*, 1–6 (2023)
- [4] Dengo, J.: The problem of gulf stream separation: A barotropic approach. *Journal of Physical oceanography* **23**(10), 2182–2200 (1993)
- [5] Chassignet, E., Marshall, D.: Gulf Stream Separation in Numerical Ocean Models. American Geophysical Union, ??? (2008)
- [6] Ezer, T.: Revisiting the problem of the gulf stream separation: on the representation of topography in ocean models with different types of vertical grids. *Ocean Modelling* **104**, 15–27 (2016)
- [7] Spall, M.A.: Dynamics of the gulf stream/deep western boundary current crossover. part i: Entrainment and recirculation. *Journal of physical oceanography* **26**(10), 2152–2168 (1996)
- [8] Zhang, R., Vallis, G.K.: The role of bottom vortex stretching on the path of the north atlantic western boundary current and on the northern recirculation gyre. *Journal of Physical Oceanography* **37**(8), 2053–2080 (2007)
- [9] Hurlburt, H.E., Hogan, P.J.: The gulf stream pathway and the impacts of the eddy-driven abyssal circulation and the deep western boundary current. *Dynamics of Atmospheres and Oceans* **45**(3-4), 71–101 (2008)
- [10] Schoonover, J., Dewar, W.K., Wienders, N., Deremble, B.: Local sensitivities of the gulf stream separation. *Journal of Physical Oceanography* **47**(2), 353–373 (2017)

- [11] Andres, M.: On the recent destabilization of the gulf stream path downstream of cape hatteras. *Geophysical Research Letters* **43**(18), 9836–9842 (2016)
- [12] Gangopadhyay, A., Gawarkiewicz, G., Silva, E.N.S., Monim, M., Clark, J.: An observed regime shift in the formation of warm core rings from the gulf stream. *Scientific reports* **9**(1), 12319 (2019)
- [13] Silver, A., Gangopadhyay, A., Gawarkiewicz, G., Fratantoni, P., Clark, J.: Increased gulf stream warm core ring formations contributes to an observed increase in salinity maximum intrusions on the northeast shelf. *Scientific Reports* **13**(1), 1–9 (2023)
- [14] Wang, J.L., Zhuang, H., Chérubin, L.M., Ibrahim, A.K., Muhamed Ali, A.: Medium-term forecasting of loop current eddy cameron and eddy darwin formation in the gulf of mexico with a divide-and-conquer machine learning approach. *Journal of Geophysical Research: Oceans* **124**(8), 5586–5606 (2019)
- [15] Agarwal, N., Kondrashov, D., Dueben, P., Ryzhov, E., Berloff, P.: A comparison of data-driven approaches to build low-dimensional ocean models. *Journal of Advances in Modeling Earth Systems* **13**(9), 2021–002537 (2021)
- [16] Chattopadhyay, A., Nabizadeh, E., Hassanzadeh, P.: Analog forecasting of extreme-causing weather patterns using deep learning. *Journal of Advances in Modeling Earth Systems* **12**(2), 2019–001958 (2020)
- [17] Chattopadhyay, A., Mustafa, M., Hassanzadeh, P., Kashinath, K.: Deep spatial transformers for autoregressive data-driven forecasting of geophysical turbulence. In: *Proceedings of the 10th International Conference on Climate Informatics*, pp. 106–112 (2020)
- [18] Chattopadhyay, A., Hassanzadeh, P.: Long-term instabilities of deep learning-based digital twins of the climate system: The cause and a solution. *arXiv preprint arXiv:2304.07029* (2023)
- [19] Dukhovskoy, D.S., Ubnoske, J., Blanchard-Wrigglesworth, E., Hiester, H.R., Proshutinsky, A.: Skill metrics for evaluation and comparison of sea ice models. *Journal of Geophysical Research: Oceans* **120**(9), 5910–5931 (2015)
- [20] Dalcher, A., Kalnay, E.: Error growth and predictability in operational ecwf forecasts. *Tellus A* **39**(5), 474–491 (1987)
- [21] DelSole, T.: Predictability and information theory. part i: Measures of predictability. *Journal of the atmospheric sciences* **61**(20), 2425–2440

(2004)

- [22] Dukhovskoy, D.S., Chassignet, E.P., Bozec, A., Morey, S.L.: Assessment of predictability of the loop current in the gulf of mexico from observing system experiments and observing system simulation experiments. *Frontiers in Marine Science* **10**, 1153824 (2023)
- [23] Weyn, J.A., Durran, D.R., Caruana, R.: Improving data-driven global weather prediction using deep convolutional neural networks on a cubed sphere. *Journal of Advances in Modeling Earth Systems* **12**(9), 2020–002109 (2020)
- [24] Krishnapriyan, A.S., Queiruga, A.F., Erichson, N.B., Mahoney, M.W.: Learning continuous models for continuous physics. arXiv preprint arXiv:2202.08494 (2022)
- [25] Li, Z., Kovachki, N., Azizzadenesheli, K., Liu, B., Bhattacharya, K., Stuart, A., Anandkumar, A.: Fourier neural operator for parametric partial differential equations. arXiv preprint arXiv:2010.08895 (2020)
- [26] Xu, Z.-Q.J., Zhang, Y., Luo, T., Xiao, Y., Ma, Z.: Frequency principle: Fourier analysis sheds light on deep neural networks. arXiv preprint arXiv:1901.06523 (2019)